Clays and Clay Minerals, Vol. 23, pp. 278–288. Pergamon Press 1975. Printed in Great Britain

CLOSED FORM EQUATIONS FOR X-RAY DIFFRACTION BY INTERSTRATIFIED CLAY SYSTEMS—I: RANDOMLY OCCURRING INTERLAMELLAR SPECIES

A. C. WRIGHT

Baroid Division of NL Industries, P.O. Box 1675, Houston, Texas 77001, U.S.A.

(*Received* 11 *February* 1975)

Abstract—A closed form equation is derived for the calculation of the oriented diffraction pattern given by single particle size layer silicates having randomly interstratified interlamellar species. A general method for treating any particle size distribution is indicated and closed form results are presented for the Poisson, normal, gamma and binomial distributions. No restriction is placed on the number of interlayer types. The structure factors for these types are explicitly introduced. Graphs of two of the variables appearing in the equations applicable to particle size distributions provide a means of visualizing the effects of both interstratification and particle size on observed X-ray patterns.

INTRODUCTION

Over the years numerous publications have appeared on the subject of the theoretical calculation of diffraction by irregularly interstratified laminar systems. The best known early paper is that by Hendricks and Teller (1942) dealing with the case of infinite crystallites. Of more interest to clay scientists, however, are treatments applicable to small particle size assemblages. Of these the matrix method of Kakinoki and Komura (1952) appears to be the most complete in that structure factors for all of the layers are introduced and varying degrees of non-random interstratification may be handled. For small particle size systems containing only a few different types of layers, the direct cosine summation method of MacEwan (1958, 1959) may be applied. Of special value as a reference work is the set of mixing function curves published in book form by Amil, Garcia and MacEwan (1967) for a wide variety of two component mixtures over the entire range of nearest neighbor interactions. MacEwan's method in somewhat modified form has been used with considerable success by Reynolds (1967) in calculating oriented diffraction patterns closely corresponding to actual diffraction runs.

Though notationally different, both the matrix and cosine summation methods ultimately involve a rather cumbersome and, even in this computer age, time consuming summation over all possible phase shifts between all of the different layer types. While this approach seems unavoidable in the general case, Méring (1949, 1950) has shown that when interstratification is random a closed form equation for the mixing function may be obtained for single particle size systems.

In the treatment which follows the case of randomly interstratified single particle size systems is also dealt with, again leading to a closed form equation. Since the structure factors for all of the layer types are explicitly introduced, the Méring equation occurs as a special case. No limit is placed on the number of interlayer species; a continuum of interlayer types may in fact be admitted by replacing certain of the necessary summations by integrals. A general method for allowing a distribution of particle sizes is given and closed form results are derived for several distributions of practical interest. The final section of this paper explores what the author believes to be a novel and conceptually valuable means of visualizing how both interstratification and particle size contribute to produce observed diffraction features.

THEORY

Consider for the moment an oriented laminar particle made up of n arbitrary layers (Fig. 1). Let the structure factor for the kth layer be denoted $F^{(k)}$. Then the amplitude of the scattered electric vector, exclusive of Lorentz polarization and other geometric or instrumental effects, is proportional to

$$A = \sum_{k=1}^{n} F^{(k)} e^{i2\pi\mu z^{(k)}},$$

where

$$\mu = 1/d = 2 \sin \theta/\lambda.$$

The scattered intensity then is proportional to

$$|A|^2 = 2\left[\sum_{k>j}^{n} F^{(k)} F^{(j)*} e^{i\varphi_{kj}}\right]_{\text{Real}} + \sum_{k=1}^{n} |F^{(k)}|^2, \quad (1)$$

where

$$\varphi_{kj} = 2\pi\mu(z^{(k)} - z^{(j)}).$$

Equation (1) applies to diffraction by a single particle of arbitrary but fixed structure. To find the average scattered intensity per particle for an assemblage of incoherently arranged particles, the equation must be averaged by taking into account the probability

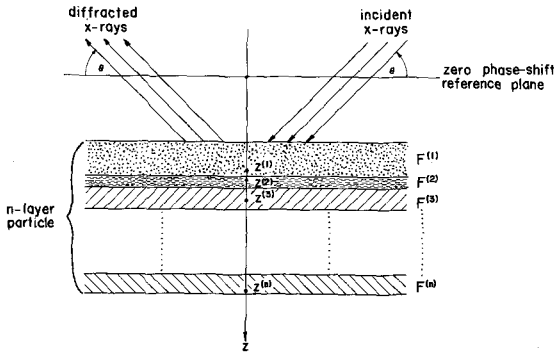

Fig. 1. Arbitrarily oriented n-layer particle. Local origin and structure factor for layer i denoted by $z^{(i)}$ and $F^{(i)}$, respectively.

of finding a given phase shift between any two types of layers.

$$|A|^2_{av} = 2\left[\sum_K \sum_L F_K F_L^* \left(\sum_{j(K,L)} P(K,L;j)\, e^{i\varphi_j}\right)\right]_{\text{Real}} + \sum_K P(K)|F_K|^2. \qquad (2)$$

The indices K and L specify which layer types while the set $\{\varphi_{j(K,L)}\}$ is all of the possible positive phase shifts between layer types K and L. $P(K, L; j)$ denotes the probable number of occurrences of phase shift φ_j and $P(K)$, the probable number of occurrences of layer type K per particle.

In what follows we shall assume that the particles consist of identical layers, referred to as basic layers, separated by different types of randomly occurring interlayer species. For clay systems the basic layers are the silicate layers while the interlayer types are the exchange ions, if any, plus any other materials which might be present between the silicate layers. The case of no interlayer material separating adjacent basic layers can be handled simply by letting the interlayer structure factor for this occurrence be zero.

Single particle size systems

Initially, assume that the assemblage is made up of particles all having the same number N of basic layers and that only two different interlayer types are present. Denote the basic layer structure factor by F_0 and the interlayer structure factors by F_1 and F_2. In addition, assume that the interlayer structure factors are evaluated at local origins located midway between the local origins of the basic layers on either side (Fig. 2). Then we have the following sets of possible phase shifts:

$$\begin{aligned}
\{\varphi_{j(0,0)}\} &= \{n\varphi_1 + m\varphi_2\} \\
\{\varphi_{j(1,1)}\} &= \{(n+1)\varphi_1 + m\varphi_2\} \\
\{\varphi_{j(2,2)}\} &= \{n\varphi_1 + (m+1)\varphi_2\} \\
\{\varphi_{j(0,1)}\} = \{\varphi_{j(1,0)}\} &= \{(n+\tfrac{1}{2})\varphi_1 + m\varphi_2\} \\
\{\varphi_{j(0,2)}\} = \{\varphi_{j(2,0)}\} &= \{n\varphi_1 + (m+\tfrac{1}{2})\varphi_2\} \\
\{\varphi_{j(1,2)}\} = \{\varphi_{j(2,1)}\} &= \{(n+\tfrac{1}{2})\varphi_1 + (m+\tfrac{1}{2})\varphi_2\}
\end{aligned}$$

where

$n + m \leqslant N - 1$
$\varphi_i = 2\pi\mu z_i$
z_i = center-to-center distance between adjacent basic layers separated by an F_i layer.

Here n and m are the numbers of F_1 and F_2 layers, respectively, which occur between the two layer types indicated in the subscripts.

For particular values of n and m we have

$$P(0,0;n,m) = \binom{n+m}{n} p_1^n p_2^m [N - (n+m)],$$

where p_i = probability of occurrence of an F_i type layer ($p_1 + p_2 = 1$). The factor

$$\binom{n+m}{n} p_1^n p_2^m$$

is the probability that exactly nF_1 layers and mF_2 layers occur in $(n + m)$ spaces regardless of order, while the last factor gives the number of ways $(n + m)$ contiguous spaces may be fitted on an N-layer particle. By summing over all possible n and m values, the contribution of $F_0 F_0^*$ terms to the bracket in equation (2) is found to be

$$F_0 F_0^* \sum_{n=0}^{N-1} \sum_{m=0}^{N-n-1} \binom{n+m}{n} p_1^n p_2^m [N-(n+m)]\, e^{i(n\varphi_1 + m\varphi_2)}.$$

For mathematical convenience the $n = m = 0$ term has been included. This may be allowed for by adding a $-2N|F_0|^2$ term to the final equation.

In considering the contribution of terms involving F_1 and F_2 some decision must be made as to the occurrence of material at the outer faces of the particles. The assumption chosen here, primarily because of the somewhat less complicated mathematics involved, is that the regions at the two faces can be treated identically to the interlayer spaces. That is, for an N-layer particle, there are $N + 1$ equivalent places where 'interlayer' types occur. The remaining probabilities in equation (2) may then be written:

$$\begin{aligned}
P(1,1;n,m) &= p_1^2 P(0,0;n,m) \\
P(2,2;n,m) &= p_2^2 P(0,0;n,m) \\
P(1,2;n,m) = P(2,1;n,m) &= p_1 p_2 P(0,0;n,m) \\
P(1,0;n,m) = P(0,1;n,m) &= p_1 P(0,0;n,m) \\
P(2,0;n,m) = P(0,2;n,m) &= p_2 P(0,0;n,m) \\
P(0) = N; P(1) = (N+1)p_1; &P(2) = (N+1)p_2.
\end{aligned}$$

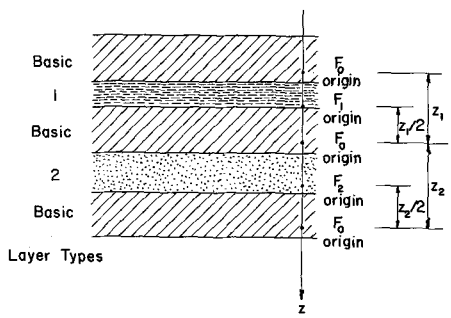

Fig. 2. Detail of particle having two interlayer types showing local origins for structure factor evaluations.

https://doi.org/10.1346/CCMN.1975.0230404 Published online by Cambridge University Press

As before, n and m designate the numbers of intervening F_1 and F_2 layers, respectively, between the two layers concerned.

Substituting all of these expressions in equation (2) and factoring results in

$$|A|^2_{av} = 2\Bigg[(F_0 + p_1F_1\,e^{i\varphi_1/2} + p_2F_2\,e^{i\varphi_2/2})(F_0^* + p_1F_1^*\,e^{i\varphi_1/2} + p_2F_2^*\,e^{i\varphi_2/2}) \times \sum_{n=0}^{N-1}\sum_{m=0}^{N-n-1}[N-(n+m)]\binom{n+m}{n}p_1^n p_2^m\, e^{i(n\varphi_1+m\varphi_2)}\Bigg]_{\text{Real}} - N|F_0|^2 + (N+1)(p_1|F_1|^2 + p_2|F_2|^2). \quad (3)$$

The negative rather than positive sign for the $|F_0|^2$ term outside of the bracket arises from the inclusion of the $-2N|F_0|^2$ term mentioned before. Note that because of the symmetry of the structure factors in equation (3) it is immaterial whether the local z-axes of the layers in any one particle are all parallel or antiparallel to the z-axis of the zero phase shift reference plane (Fig. 1). Even if the structure factors have imaginary components, an "up-side-down" particle gives on the average the same diffracted intensity as a "right-side-up" one. Within each particle, however, all local z-axes must have the same sense; otherwise there would be, in effect, double the number of layer types.

By transforming the indices in equation (3), the double summation is found to reduce to two geometric series.

$$\text{Double sum} = \sum_{r=0}^{N-1}(N-r)\sum_{t=0}^{r}\binom{r}{t}(p_1\,e^{i\varphi_1})^{r-t}(p_2\,e^{i\varphi_2})^t$$
$$= N\sum_{r=0}^{N-1}\alpha^r - \sum_{r=0}^{N-1}r\alpha^r$$
$$= N/(1-\alpha) - \alpha(1-\alpha^N)/(1-\alpha)^2,$$

where

$$\alpha = p_1\,e^{i\varphi_1} + p_2\,e^{i\varphi_2}.$$

Therefore, for an assemblage of N-layer particles, the average diffracted intensity per particle is proportional to

$$|A|^2_{av} = 2\left[\beta\beta^\dagger\left(\frac{N}{1-\alpha} - \frac{\alpha(1-\alpha^N)}{(1-\alpha)^2}\right)\right]_{\text{Real}} - N|F_0|^2 + (N+1)\gamma \quad (4)$$

where

$$\beta = F_0 + p_1F_1\,e^{i\varphi_1/2} + p_2F_2\,e^{i\varphi_2/2},$$

denotes the operation of changing each structure factor, but not its associated phase shift multiplier, to its complex conjugate, and

$$\gamma = p_1|F_1|^2 + p_2|F_2|^2.$$

When a derivation analogous to the above is made for more than two interlayer types, equation (4) again results in exactly the same form: α, β and γ need only be modified by adding the appropriate terms. In this case a multinomial, rather than binomial, expansion involving the phase shifts is found when equation (2) is explicitly written out. In the limit of an infinite number of infinitesimally differing interlayer types, a continuum of species may be admitted by use of integrals in calculating the required α, β and γ variables. Specifically,

let

$$\alpha = \sum_{k=1}^{M} p_k\,e^{i\varphi_k} + \int P(\xi)\,e^{i\varphi(\xi)}\,d\xi$$

$$\beta = F_0 + \sum_{k=1}^{M} p_kF_k\,e^{i\varphi_k/2} + \int P(\xi)F(\xi)\,e^{i\varphi(\xi)/2}\,d\xi$$

and

$$\gamma = \sum_{k=1}^{M} p_k|F_k|^2 + \int P(\xi)|F(\xi)|^2\,d\xi,$$

where

M = number of discrete types,
ξ is the continuum parameter,
F_k is the structure factor for discrete interlayer type k,
$F(\xi)$ is the structure factor for continuum interlayer type ξ,
φ_k and $\varphi(\xi)$ are the phase shifts between adjacent basic layers when interlayer types k and ξ intervene, respectively,
$P(\xi)$ is the continuum probability density function,

and

$$\sum_{k=1}^{M} p_k + \int P(\xi)\,d\xi = 1.$$

Then the insertion of these variables into equation (4) gives the desired diffraction intensity. The examples given in the Applications section of this paper should make clear the construction of the α, β and γ variables for any particular case.

Extension to particle size distributions

In common with other single particle size calculations of this sort, equation (4) gives rise to interference fringes associated with sharp diffraction peaks. A more realistic approach which serves to attenuate or eliminate these fringes is to introduce a particle size distribution and suitably average equation (4). Let the probability that a given particle in the assemblage have N basic layers be denoted $\mathscr{P}(N)$. Then

$$\sum_{N=0}^{\infty}\mathscr{P}(N) = 1 \quad \text{and} \quad \sum_{N=0}^{\infty}N\mathscr{P}(N) = \bar{N},$$

where $\bar{N}$ is the average particle size. The case $N = 0$ is included merely for mathematical convenience as many useful normalized distributions have non-zero values for $\mathscr{P}(0)$.

Since equation (4) gives the average intensity per N-layer particle, we have

$$|A|^2_{av} = \sum_{N=1}^{\infty}\mathscr{P}(N)|A|^2_{N,av} \quad (5)$$
$$= 2[\beta\beta^\dagger B(\alpha)]_{\text{Real}} - \bar{N}|F_0|^2 + (\bar{N} + 1 - \mathscr{P}(0))\gamma,$$

https://doi.org/10.1346/CCMN.1975.0230404 Published online by Cambridge University Press

where

$$B(\alpha) = \bar{N}/(1-\alpha) - \alpha(1-\tau)/(1-\alpha)^2$$

and

$$\tau = \sum_{N=0}^{\infty} \mathscr{P}(N)\alpha^N.$$

Often the interlayer structure factors are negligible in comparison to the basic layer structure factor. For this approximation then $\beta = F_0$ and $\gamma = 0$. The basic layer structure factor is seen to be separable, and a pure "mixing function", $\Phi(\mu)$, results.

$$\Phi(\mu) = \frac{|A|^2_{\text{av}}}{|F_0|^2} = 2B(\alpha)_{\text{Real}} - \bar{N} \qquad (6)$$

The function $B(\alpha)$ which is defined in equation (5) appears to have a singularity at $\alpha = 1$. Combining its terms over the common denominator $(1-\alpha)^2$, however, shows the numerator to likewise have a second order zero at this point. A practical consequence of this behavior is the loss of significant digits when α is close to one. Thus a Taylor expansion for $B(\alpha)$ about $\alpha = 1$ will be of use for actual calculations in the immediate neighborhood of $\alpha = 1$. Straightforward application of algebraic techniques shows the coefficients of this expansion to be

$$b_n = \sum_{N=n+1}^{\infty} \binom{N+1}{n+2} \mathscr{P}(N), \qquad (7)$$

where

$$B(\alpha) = \sum_{n=0}^{\infty} b_n(\alpha - 1)^n.$$

When the binomial factors are explicitly written out, the leading terms are found to be $b_0 = (\overline{N^2} + \bar{N})/2$ and $b_1 = (\overline{N^3} - \bar{N})/6$. As one would anticipate from general principles, the mixing function in equation (6) is seen to have a value of $\overline{N^2}$ at the principle diffraction maximum ($\alpha = 1$).

Diffraction by assemblages containing but one kind of interlayer species is also described by equations (5) and (6) since obviously we may set p_1 equal to one. Note, however, that equation (5) still applies to N-layer particles having $N+1$ "interlayer" regions. If the usual approximation is made that end effects can be ignored, then the interlayer structure factor can be included in the basic layer structure factor and equation (6) applied. For this case the mixing function simply generates the diffraction line profile $D(\mu)$ characteristic of the particle size distribution assumed. Because $|\alpha| = 1$ for all μ, equation (6) may be simplified to give

$$D(\mu) = (1 - \tau_{\text{Real}})/(1\text{-cos}\varphi), \qquad (8)$$

where

$$\varphi = 2\pi\mu d(001).$$

Specific distributions

Use of equations (5) and (6) requires evaluation of the variable τ which is itself dependent on the particle size distribution assumed. If the distribution is relatively narrow, directly carrying out the indicated sum over all non-negligible $\mathscr{P}(N)$ is feasible. For certain distributions, however, closed forms for τ as a function of both α and the distribution parameters may be derived.

As an example, consider the Poisson distribution which is defined by the equation

$$\mathscr{P}(N) = e^{-\bar{N}}(\bar{N})^N/N!$$

where

$$N = 0, 1, 2, \ldots$$

Substituting these values for $\mathscr{P}(N)$ in the general expression for τ gives

$$\tau = e^{-\bar{N}} \sum_{N=0}^{\infty} (\bar{N}\alpha)^N/N! = e^{\bar{N}(\alpha-1)}.$$

By transforming the summation index in equation (7) so that the new index starts at zero, the b_n coefficients in the $B(\alpha)$ expansion for the Poisson distribution are found to be

$$b_n = (\bar{N})^{n+1}(\bar{N} + n + 2)/(n+2)!$$

These results are summarized in Table 1.

Also presented in Table 1 are similar results which have been derived for the normal, gamma and binomial distributions. Note that the two parameters of the normal and gamma distributions allow specification of the first two distribution moments. The form of the binomial distribution, having three independent parameters, allows specification of the first three.

In order to obtain closed forms for τ in the cases of the normal and gamma distributions, it was necessary to replace the summations by integrals. While this approximation seems severe, particularly for small particle sizes, in practice it works quite well. As an example, the four place printout of an exact calculation involving a normal distribution with $\bar{N} = 5$ and $\sigma^2 = 1$ truncated at $N = 1$ and 9 differed not at all from that for a similar calculation utilizing the integral approximation. The principle diffraction maximum at $\alpha = 1$ had in both instances been normalized to one.

Infinite crystallites

From equation (4), which gives the diffracted intensity for single particle size assemblages, it is a simple matter to find the form of the working equations for infinite crystallites. To obtain a finite limit as N goes to infinity, division of both sides of the equation by N is necessary to get the intensity per basic layer rather than per particle. For large N the second term in the bracket is seen to go to zero while the γ multiplier goes to one, thus giving

$$|A|^2_{\text{inf}} = 2[\beta\beta^{\dagger}/(1-\alpha)]_{\text{Real}} - |F_0|^2 + \gamma. \qquad (9)$$

If the mixing function approximations are applied, there results

$$\Phi(\mu)_{\text{inf}} = 2[1/(1-\alpha)]_{\text{Real}} - 1. \qquad (10)$$

The final equation in Section 2 of the paper by Hendricks and Teller (1942), though more complicated

https://doi.org/10.1346/CCMN.1975.0230404 Published online by Cambridge University Press

Table 1. Summary of closed form results for τ and $B(\alpha)$ expansion coefficients for various distributions

Def.: $\tau = |\tau| e^{i\eta}$ and $\alpha = |\alpha| e^{i\varphi} = x + iy$

where $-\pi \leqslant \varphi \leqslant \pi$ and x and y are real

A. Single particle size

$\mathscr{P}(N) = 1$ for $N = \bar{N}$
$= 0$ otherwise

$\tau = \alpha^{\bar{N}}$
$|\tau| = |\alpha|^{\bar{N}}$
$\eta = \bar{N}\varphi$
$b_0 = \bar{N}(\bar{N} + 1)/2$
$b_1 = \bar{N}(\bar{N}^2 - 1)/6$

B. Poisson distribution

$\mathscr{P}(N) = e^{-\bar{N}}\bar{N}^N/N!$
$N = 0, 1, 2, \ldots$

$\tau = e^{\bar{N}(\alpha-1)}$
$|\tau| = e^{\bar{N}(x-1)}$
$\eta = \bar{N}y$
$b_0 = \bar{N}(\bar{N} + 2)/2$
$b_1 = \bar{N}^2(\bar{N} + 3)/6$

C. Normal distribution (integral approximation)

$$\mathscr{P}(N) = \frac{1}{\sqrt{(2\pi)}\sigma} e^{-(N-\bar{N})^2/2\sigma^2}$$
$$N = \ldots, -1, 0, 1, 2, \ldots$$

where $\bar{N}$ and σ are such that $\mathscr{P}(N < 0)$ is negligible.

$\tau = \alpha^{\bar{N}} e^{(\sigma \ln \alpha)^2/2}$
$|\tau| = |\alpha|^{\bar{N}} e^{\sigma^2(\ln^2|\alpha| - \varphi^2)/2}$
$\eta = \varphi(\bar{N} + \sigma^2 \ln|\alpha|)$
$b_0 = [\bar{N}(\bar{N} + 1) + \sigma^2]/2$
$b_1 = \bar{N}(\bar{N}^2 - 1 + 3\sigma^2)/6$

D. Gamma distribution (integral approximation)

$$\mathscr{P}(N) = \frac{1}{\epsilon^k \Gamma(k)} N^{k-1} e^{-N/\epsilon} \quad N = 0, 1, 2, \ldots$$

where $\epsilon = \overline{(N - \bar{N})^2}/\bar{N} = \overline{N^2}/\bar{N} - \bar{N}$ and $k = \bar{N}/\epsilon$.

$\tau = 1/(1 - \epsilon \ln \alpha)^k$
$|\tau| = 1/[(1 - \epsilon \ln|\alpha|)^2 + (\epsilon\varphi)^2]^{k/2}$
$\eta = k \tan^{-1}[\epsilon\varphi/(1 - \epsilon \ln|\alpha|)]$
$b_0 = k\epsilon[(k + 1)\epsilon + 1]/2$
$b_1 = k\epsilon[(k + 1)(k + 2)\epsilon - 1]/6$

E. Binomial distribution*

$$\mathscr{P}(N) = \binom{R}{N - S} p^{N-S} q^{R+S-N}$$
$$N = S, S + 1, \ldots, S + R$$

where $p = (\bar{N} - S)/R$, $q = 1 - p$, $\overline{(N - \bar{N})^2} = Rpq$ and $\overline{(N - \bar{N})^3} = Rpq(q - p)$.

$\tau = \alpha^S(p\alpha + q)^R$
$|\tau| = |\alpha|^S[(px + q)^2 + (py)^2]^{R/2}$
$\eta = S\varphi + R \tan^{-1}[py/(px + q)]$
$b_0 = [\bar{N}(\bar{N} + 1) + Rpq]/2$
$b_1 = [\bar{N}(\bar{N}^2 - 1) + Rpq(q - p + 3\bar{N})]/6$

* Derived results also apply to more general beta distribution (S and $R + S$ not necessarily integral).

in appearance, can be shown to be mathematically identical to equation (10).

APPLICATIONS

By this point the reader may well be somewhat overwhelmed by the number of different variables which have been introduced. In actual practice, however, these variables serve to break the problem into various independent and fairly simple parts. A stepwise procedure for a complete calculation using equation (5) might be the following.

Given μ;
(1) evaluate $\alpha(\mu)$,
(2) calculate $\tau(\alpha)$; functional form is dependent on particle size distribution,
(3) evaluate $B(\alpha, \tau)$; use expansion for α close to one,
(4) calculate structure factors; all interlayer structure factors must be calculated with respect to local origins located midway between the local origins of the basic layers on either side,
(5) evaluate β and $\beta^\dagger$, then form product $\beta\beta^\dagger$; if all structure factors are real then $\beta = \beta^\dagger$,
(6) calculate γ,
(7) insert γ, $|F_0|^2$ and real part of $\beta\beta^\dagger B(\alpha)$ into equation (5) and
(8) apply Lorentz and geometric factors to result.

Thus, in a computer program, the evaluation of α, τ, $B(\alpha)$, the structure factors, $\beta\beta^\dagger$, and γ might each be carried out by separate short subroutines. The function of the main program would be simply to organize the input data for use by the subroutines and to combine the various results in step (7).

The range of application of the equations which have been derived is surprisingly broad because of the simple additive construction of the α, β and γ variables. It is hoped that the few examples given in this section will demonstrate this versatility. In all cases the mixing function approximation has been used in preparing the figures so that structure factor effects do not mask those arising from mixed layering. Calculations for the figures were performed on a Model 9820A Hewlett-Packard calculator, a programmable desk top computer of modest memory size and speed. Typically one to two seconds were required per data point. A two term expansion for $B(\alpha)$ was used when $|\alpha - 1| < 0{\cdot}01$.

Discrete interlayer types

Consider a partially hydrated 2:1 clay having a random mixture of spacings corresponding to zero, one and two water layers separating adjacent silicate layers. For the purposes of this calculation, we shall assume these spacings to be 9·5, 12·5 and 15·5 Å, respectively. The basic layer is taken to be the 2:1 layer exclusive of exchange ions. If the interlayer structure factors are denoted by their characteristic spacings, then $F(9{\cdot}5)$ is the structure factor for the anhydrous exchange ions while $F(12{\cdot}5)$ and $F(15{\cdot}5)$ include the scattering by one and two water layers, respectively. Since each type of layer has a center of symmetry, the structure factors may all be evaluated with respect to these centers.

The α, β and γ variables for this three component case are

$$\alpha = p(9{\cdot}5)\, e^{i19\pi\mu} + p(12{\cdot}5)\, e^{i25\pi\mu} + p(15{\cdot}5)\, e^{i31\pi\mu},$$

$$\beta = F(2{:}1) + p(9{\cdot}5)F(9{\cdot}5)\, e^{i9{\cdot}5\pi\mu} + p(12{\cdot}5)F(12{\cdot}5)\, e^{i12{\cdot}5\pi\mu} + p(15{\cdot}5)F(15{\cdot}5)\, e^{i15{\cdot}5\pi\mu},$$

$$\beta^\dagger = \beta,$$

https://doi.org/10.1346/CCMN.1975.0230404 Published online by Cambridge University Press

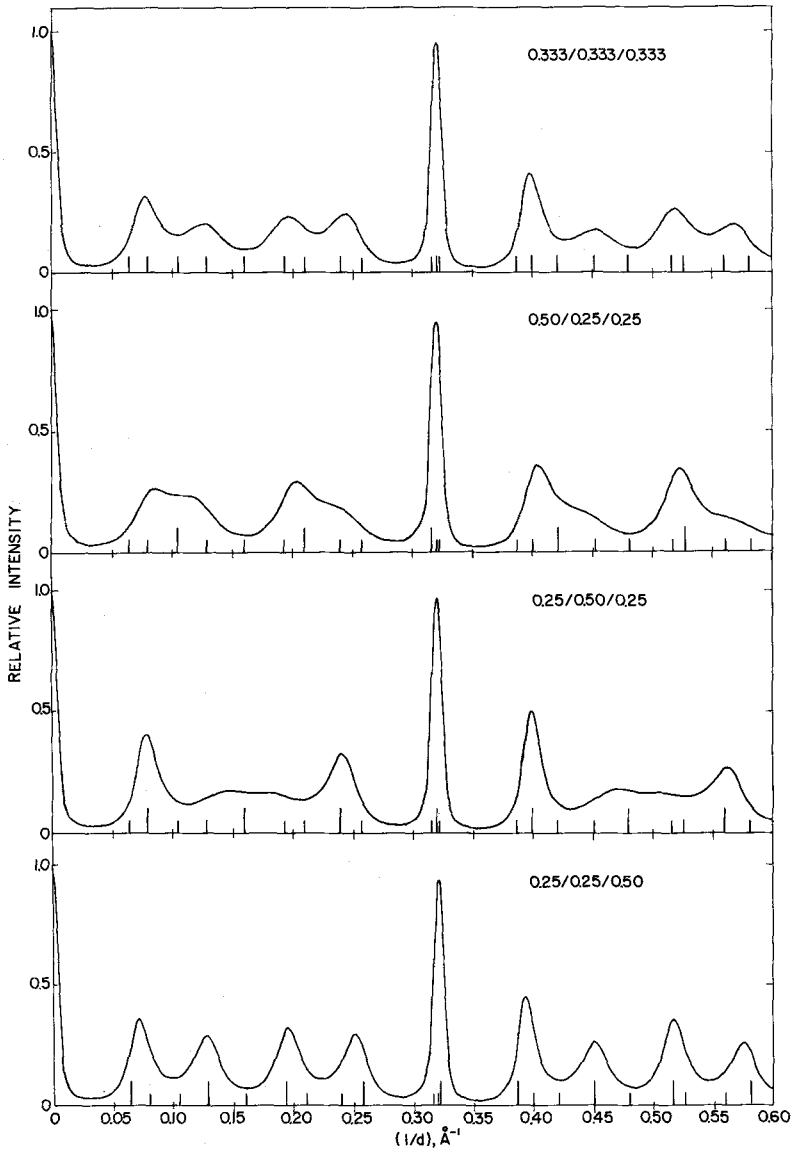

Fig. 3. Calculated intensity vs μ for three component mixture. Probabilities given as $p(9{\cdot}5)/p(12{\cdot}5)/p(15{\cdot}5)$. Five layer Poisson distribution.

and

$$\gamma = p(9{\cdot}5)|F(9{\cdot}5)|^2 + p(12{\cdot}5)|F(12{\cdot}5)|^2 + p(15{\cdot}5)|F(15{\cdot}5)|^2.$$

Figure 3 shows mixing function calculations for four sets of probabilities. A Poisson particle size distribution with $\bar{N} = 5$ was assumed. The small vertical lines along each μ axis denote the positions where the basal lines would occur for the pure components. It is of some practical interest to note that, due to the near coincidence of the higher order basal lines of all three components near $\mu = 0{\cdot}32$, a sharp peak is always observed in this region even when mixed layering greatly broadens other features. This effect has in fact been observed by Rowland, Weiss and Bradley (1956) in their diffraction studies of heated clay films.

A continuum of interlayer types

Given the partially random nature of isomorphous substitution in expansible 2:1 clays, it is reasonable to expect small variations in spacing between adjacent silicate layers, particularly when sorbed interlayer species are present. If these variations occur randomly along the z-axis, then the equations developed here may be applied to determine how this disorder effects the basal diffraction pattern.

Assume that the center to center spacing between adjacent 2:1 layers, D, has a normal distribution

$$P(D) = \frac{1}{\sqrt{(2\pi)}\Delta} e^{-(D-z_0)^2/2\Delta^2},$$

where

z_0 = average spacing
= apparent $d(001)$

https://doi.org/10.1346/CCMN.1975.0230404 Published online by Cambridge University Press

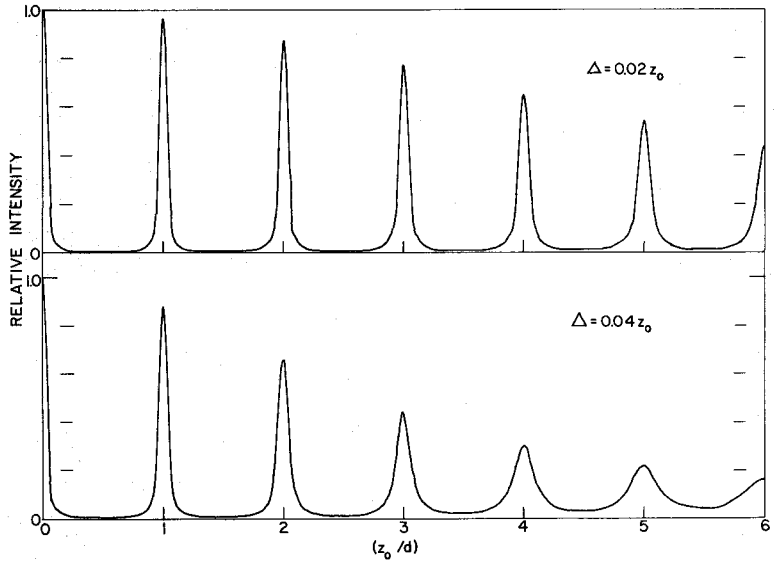

Fig. 4. Calculated intensity vs μ for normal continuum of interlayer spacings. Ten layer Poisson distribution.

and

$$\Delta \ll z_0.$$

Then, by taking D to be the continuum parameter, we have

$$\alpha = \int_{-\infty}^{+\infty} P(D)\, e^{i2\pi\mu D}\, dD = e^{-2(\pi\mu\Delta)^2}\, e^{i2\pi\mu z_0},$$

$$\beta = F(2{:}1) + \int_{-\infty}^{+\infty} P(D)F(D)\, e^{i\pi\mu D}\, dD$$

$$\doteq F(2{:}1) + F(z_0)\, e^{-(\pi\mu\Delta)^2/2}\, e^{i\pi\mu z_0},$$

$$\beta^{\dagger} = \beta,$$

and

$$\gamma = \int_{-\infty}^{+\infty} P(D)|F(D)|^2\, dD \doteq |F(z_0)|^2.$$

In deriving β and γ, the simplifying assumption has been made that the variation in the interlayer structure factor, $F(D)$, is small enough that the average interlayer structure factor, $F(z_0)$, may be substituted.

In Fig. 4 mixing function calculations for two different Δ/z_0 ratios are plotted. This condition is analogous to strain broadening in metals. Qualitatively it is seen that the presence of a continuum of interlayer types results in a gradual loss of scattering coherence as μ increases and that the greater the distribution of interlayer spacings, the more rapid is the loss of sharpness in the diffraction features. The decrease of peak intensity with increasing μ differs from that caused by temperature effects in that the integrated intensity of each peak remains very nearly constant rather than suffering an exponential decrease with μ^2.

When Δ is small compared to z_0, the principle diffraction maximum at $\mu = 0$ has a line shape almost identical to that calculated for the same particle size distribution without interlayer disorder. Even though this line is not observable in practice, any parameter relating to its shape may be determined by an extrapolation of the parameter values for the higher order peaks.

In particular, for the two plots given in Fig. 4, the width at half-height of the zero order line falls on an extrapolated graph of line width vs diffraction order squared for the higher order (observable) peaks. By using the square of the order as the abscissa, a nearly linear graph having only slight upward curvature results. Though space limitations prevent a fuller development of this subject here, it is clear that information concerning both the particle size distribution and degree of interlayer disorder is recoverable from such graphs.

A mixture of discrete and continuous interlayer types

A possible model for a partially dehydrated 2:1 clay would involve a mixture of 9·5 and 12·5 Å spacings with an added continuum of intermediate spacings. While it might be argued with some justification that the adjacent layers would no longer be strictly parallel, a calculation using this model should none the less provide some insight into the effect of such transitional regions on the oriented diffraction pattern.

Assume that the continuum probability density is constant; that is

$$P(D) = p(tr.)/(12{\cdot}5\text{–}9{\cdot}5)$$

where

$p(tr.)$ = total probability that a given spacing lies in the continuum range $9{\cdot}5 < D < 12{\cdot}5$.

Then

$$\alpha = p(9{\cdot}5)\, e^{i19\pi\mu} + p(12{\cdot}5)\, e^{i25\pi\mu} + \int_{9\cdot5}^{12\cdot5} P(D)\, e^{i2\pi\mu D}\, dD$$

$$= \left[p(9{\cdot}5) + \frac{i}{6\pi\mu}p(tr.)\right] e^{i19\pi\mu} + \left[p(12{\cdot}5) - \frac{i}{6\pi\mu}p(tr.)\right] e^{i25\pi\mu}.$$

https://doi.org/10.1346/CCMN.1975.0230404 Published online by Cambridge University Press

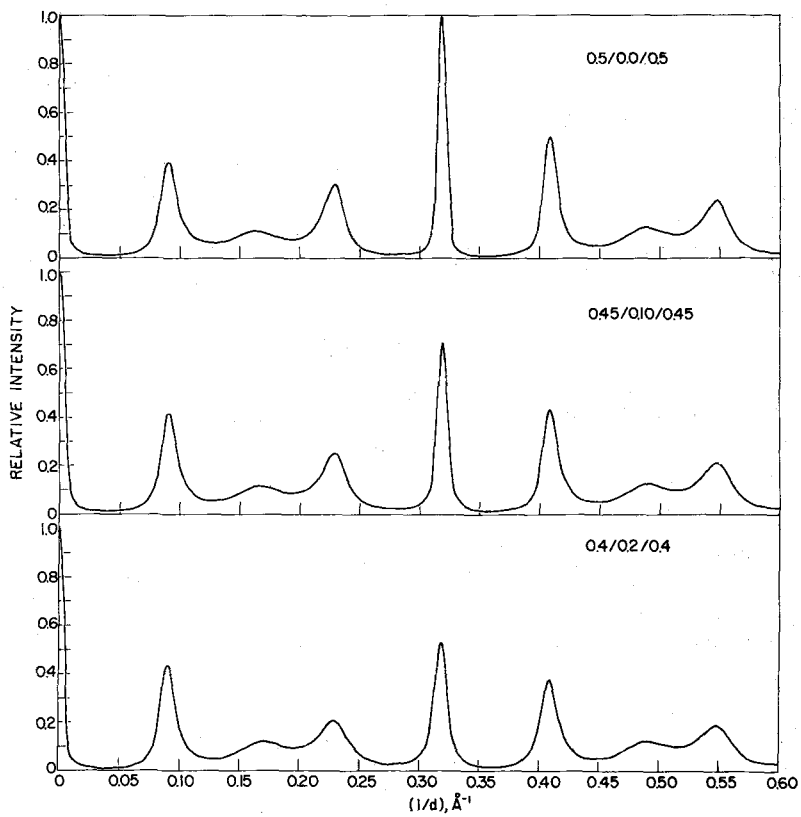

Fig. 5. Calculated intensity vs μ for two component mixture with added constant probability of transitional spacings. Probabilities given as $p(9{\cdot}5)/p(tr.)/p(12{\cdot}5)$. Eight layer Poisson distribution.

The form of the β and γ variables will depend on the interlayer structure factor used for the transitional region.

Figure 5 shows mixing function curves for equal amounts of the two discrete components with $p(tr.) =$ 0·0, 0·1 and 0·2. It is seen that the major effect of the transitional components is to decrease the sharpness and maximum intensity of the strong peak at $\mu = 0{\cdot}32$. Generally speaking the latter two patterns for large μ resemble calculations for the two discrete spacings with a somewhat smaller particle size. Why this is so will be dealt with in the final section of this paper concerning the $B(\alpha)$ map.

Particle size estimates for one-component systems

If a reasonable model for the particle size distribution of a one-component system is known, then by use of equation (8) a series of profiles may be calculated to find the parameters which give the best agreement with the observed line profile (after correction for structure factor effects, K–α doubling, etc.). Of the distributions discussed here, the simplest from this standpoint is the Poisson since it contains but one adjustable parameter.

Figure 6 shows the profiles given by the Poisson distribution for a variety of average particle sizes. Over the range shown, the widths at half-height (measured from zero diffracted intensity) are given to within one percent by the equation

$$W = \frac{0{\cdot}87}{(\bar{N} + 1{\cdot}5)d(001)},$$

where W is the width measured in units of μ.

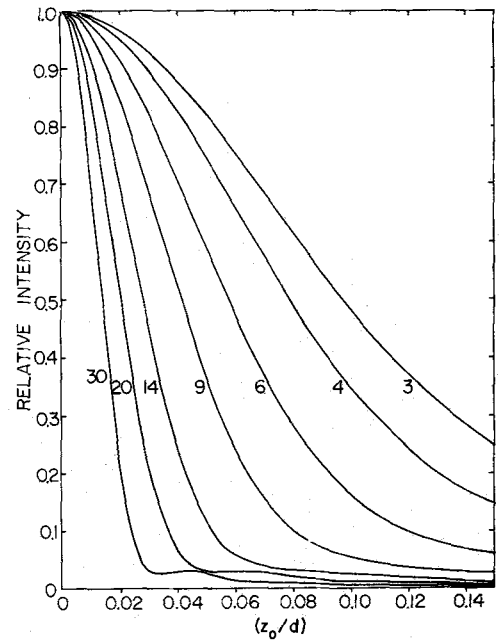

Fig. 6. Poisson distribution diffraction profiles for various average particle sizes.

https://doi.org/10.1346/CCMN.1975.0230404 Published online by Cambridge University Press

Since the first order basal lines of layer silicates occur at low enough angles that $\sin\theta \approx \theta$ and $\cos\theta \approx 1$, a good estimate of the average number of layers making up a coherent diffracting unit is given by

$$\bar{N} = 0{\cdot}87\frac{(2\theta)_{001}}{(\Delta 2\theta)_{001}} - 1{\cdot}5,$$

where

$(2\theta)_{001}$ = (001) diffraction angle,

and

$(\Delta 2\theta)_{001}$ = angular width at half-height of (001) peak.

THE $B(\alpha)$ MAP

Though a discussion of the $B(\alpha)$ function defined in equation (5) might more logically be a part of the theoretical section of this paper, it has been deferred until now in order to include the examples given in the previous section. The discussion will center on the mixing function case (equation 6) where the diffracted intensity is given within a constant simply by twice the real part of $B(\alpha)$. Even if the mixing function approximations are not applied in an actual calculation, this case is conceptually quite useful because the interlayer structure factors generally make only a minor contribution to the final calculated pattern.

For the moment it is useful to forget the original definition of the α variable and consider $B(\alpha)$ just to be a function defined in the complex plane. Given any particle size distribution we may calculate contour maps of the real and imaginary parts of $B(\alpha)$ on the (x, y) plane, where $\alpha = x + iy$. Since, in an actual calculation, α is confined to the unit circle, the behavior of $B(\alpha)$ in this region is of the most interest.

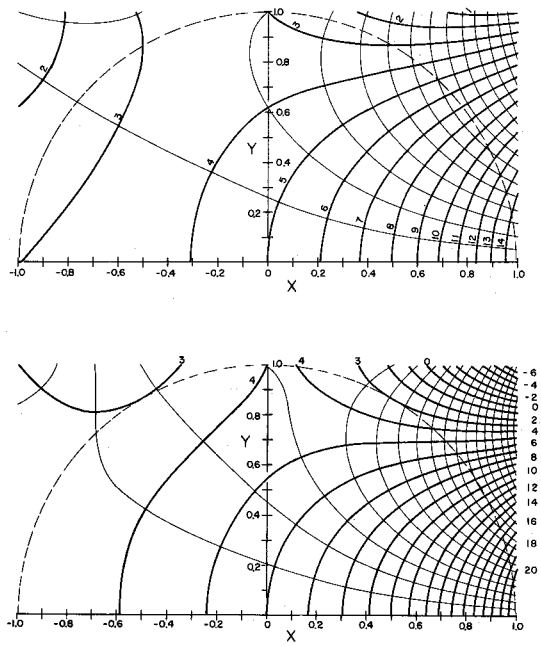

Fig. 7. $B(\alpha)$ maps for five (top) and six (bottom) layer single particle size distributions. Heavy lines are contours of real part and light lines, of imaginary part (unit contour intervals).

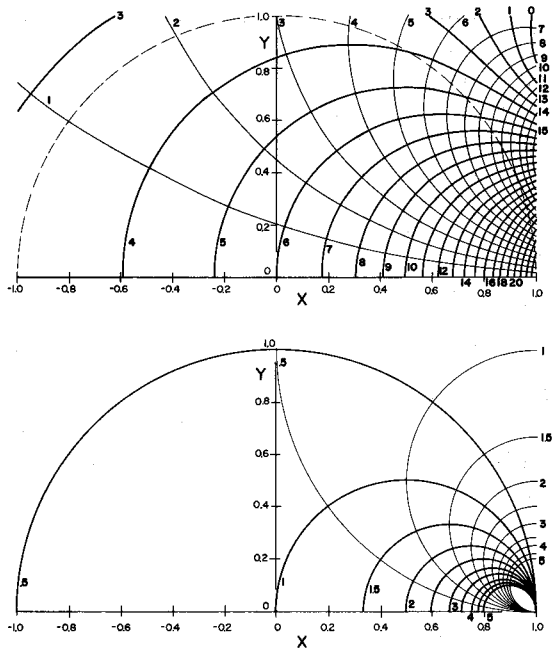

Fig. 8. $B(\alpha)$ maps for 6-layer Poisson distribution (top) and for infinite particles (bottom). Heavy lines are contours of real part and light lines, of imaginary part.

Figures 7 and 8 show such calculations for four different distributions. In all cases the real and imaginary parts have been superpositioned since the contours of one are the lines of steepest descent of the other (a general property of analytic complex functions). Only the positive y half-plane is shown since the real part of $B(\alpha)$ is symmetric and the imaginary part antisymmetric about the x-axis. In particular Fig. 7 shows maps for 5 and 6-layer single particle size "distributions", while Fig. 8 applies to a 6-layer Poisson distribution and to infinite crystallites. It is remarkable how similar the general features of the maps are, considering the differences in the distributions. Within the unit circle the real part of each increases to a maximum as α approaches one. Away from $\alpha = 1$ the slope decreases and becomes comparatively gentle for negative x. The saddle-points evidenced in the single particle size maps are seen to average out to nearly circular contours in the Poisson map. (The maps are additive since τ is itself additive.) In the map for infinite crystallites the contours are perfect circles.

The most important point to be made here is that no reference has been made to any particular mixed layer types in constructing these maps. They are defined entirely by the particle size distribution.

Now return to the original definition of the α variable. Given a specific case of mixed layering we have

$$\alpha = \sum_k p_k e^{i\varphi_k} + \int P(\xi)\, e^{i\varphi(\xi)}\, d\xi,$$

where

$$(1)\quad \varphi_k = 2\pi\mu z_k; \quad \varphi(\xi) = 2\pi\mu z(\xi)$$

and

$$(2)\quad \sum_k p_k + \int P(\xi)\, d\xi = 1.$$

https://doi.org/10.1346/CCMN.1975.0230404 Published online by Cambridge University Press

Thus, α can be constructed by plotting end-to-end its vector components on the complex plane. The discrete types when plotted give a broken line while the continuous types give a curve (the limit of an end-to-end plot of vectors of length $P(\xi)\Delta\xi$ and phase $\varphi(\xi)$ as $\Delta\xi$ goes to zero). Condition (1) expresses the fact that the value of μ determines how the end-to-end construction will be folded; condition (2) requires that the total length along the construction remain one regardless of μ.

For a specific set of interlayer types and probabilities, α becomes a function of μ only without reference to particle size. For each specification the curve that α traces out on the complex plane as μ varies may be plotted. For later reference the curve may be marked in equal increments of μ. The curve starts out in every case at $\alpha = 1$ for $\mu = 0$ and because of condition (2), is confined to the unit circle.

The independence of the $B(\alpha)$ map from specific interlayer species and of the α-plot from particle size considerations have been stressed to make clear that all that is required for a calculation involving a given set of interlayer types for a particular particle size distribution is a superposition of the appropriate graphs. The conceptual value of this observation will hopefully be made plain by the following examples.

The simplest case is that of a single component system. Here $\alpha = e^{i\varphi}$. α is constrained to move uniformly on the unit circle with angular velocity proportional to $d(001)$. In effect α picks out that curve on the $B(\alpha)$ surface which gives $D(\mu)$, the diffraction profile function. Conversely, the Poisson diffraction profile given in Fig. 6 in the Applications Section for $\overline{N} = 6$ is linearly related to the unit circle cut of the $B(\alpha)$ map in Fig. 8. In the case of the map for infinite crystallites, also given in Fig. 8, the unit circle is simply the 0·5 contour level. This value gives zero diffracted intensity for all μ as it should (except at $\varphi = 0$, where $B(\alpha)$ is undefined). For the six layer single particle size distribution (Fig. 7), the unit circle is tangent to the 3·0 contour level at $\varphi = \pi/3$, $2\pi/3$ and π, thus giving zero values for $\Phi(\mu)$ at these points. As a consequence, subsidiary maxima are observed in the diffraction profile for this distribution.

Now consider the case of more than one discrete component. Here the construction of α results in a broken line because of the differing phase angles of its various components. Initially at $\mu = 0$ all of the component vectors are aligned and the calculated intensity has its maximum value. As μ increases α must depart from the unit circle and describe a series of loops. As one would intuitively expect, the more closely the component angular velocities (i.e. basal spacings) match, the more nearly the α-plot initially resembles that of a one-component system. To a fairly good approximation, regardless of the particle size distribution considered, the calculated diffraction pattern has maxima where the loops are closest to $\alpha = 1$ and minima where the loops are furthest from this point. Only if the loops quite closely approach $\alpha = 1$ are sharp peaks observed even in the case of infinite

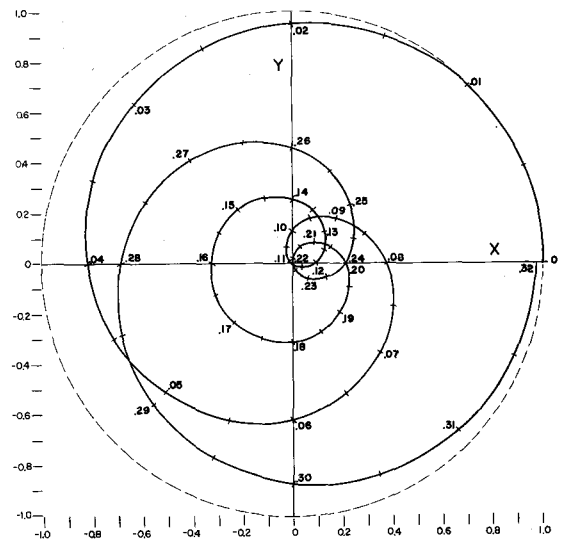

Fig. 9. α-plot for $p(9·5)/p(12·5)/p(15·5) = 0·333/0·333/0·333$. Values of μ are noted on curve.

crystallites. In addition it is clear that the ratios of the component spacings must be rational in order for the pattern ever to repeat.

Figure 9 is an α-plot for the equi-probable three component mixture discussed in the first part of the Applications Section. All of the points mentioned above can be verified by a careful comparison of this α-plot with the calculated diffraction pattern in Fig. 3. Note that, even without going to the rather extensive labor of constructing a $B(\alpha)$ map, it is possible to extract a great deal of semi-quantitative information just from the α-plot.

The limit of an infinitely large number of discrete components with only infinitesimally differing spacings defines the continuum case. Again, at $\mu = 0$ the construction of α is a straight line along $\varphi = 0$. As μ increases, however, the line must become increasingly bowed due to the smooth variation in the angular velocities of the infinitesimal components. Since there is no way the slower moving components can ever catch up with the faster ones, it is obvious that α must become zero in the limit as μ goes to infinity. The constant length vector construction of α simply winds itself up more and more tightly around the origin. The calculated intensity thus approaches that expected for $\overline{N}$ incoherently scattering layers.

As an example of this behavior we may look at the normal distribution continuum discussed in the second part of the Applications section. Examination of the formula derived there shows α to trace out a spiral which descends upon the origin. The greater the distribution of spacings (i.e. Δ), the more rapid is the approach to zero.

When both discrete and continuous components are present, again, the continuous components eventually wind themselves up and become effectively zero in length. In the third part of the Applications section dealing with this case note how the integral contributions to α drop out for large μ due to the presence

https://doi.org/10.1346/CCMN.1975.0230404 Published online by Cambridge University Press

of the $1/\mu$ factors. In general, after a certain point the pattern is determined almost entirely by the discrete components. Since the sum of the discrete probabilities is necessarily less than one, α is also now confined to a circle of radius less than one. A consideration of the general changes in the $B(\alpha)$ map with particle size shows that the calculated pattern for this reduced circle closely resembles the pattern one would calculate for the same discrete components with renormalized probabilities but with a smaller average particle size.

(As an aside, it might be noted here that quite reasonable looking 'small particle size' calculations may be made using the comparatively simple infinite crystallite equations (9) and (10) just by scaling down α. By use of a scale factor, the singular point for $B(\alpha)$ at $\alpha = 1$ is thus avoided. A scale factor close to one gives a pattern typical of large crystallites, while a smaller scale factor causes the peaks to broaden in a manner characteristic of small particles. For one-component systems the peak shape resulting from this device is very nearly Lorentzian.)

Unfortunately, a great deal of the conceptual simplicity hopefully brought out in this section is lost when the scattering contributed by the interlayer materials cannot be ignored. In this case, the imaginary component of $\beta\beta^{\dagger}$ forces a consideration of the imaginary as well as the real part of $B(\alpha)$. Contrary to what one might suppose, $\beta\beta^{\dagger}$ cannot be reasonably approximated by the squared magnitude of any sort of average structure factor. The foregoing remarks concerning the independence of $B(\alpha)$ from specific interlayer types and α from particle size still hold true however.

CONCLUSIONS

Though the mathematics involved in calculating the diffraction patterns given by randomly interstratified clay systems is not trivial, the approach developed here, leading to the concepts of the $B(\alpha)$ map and the α-plot, allows a penetrating visualization of how specific interlayer spacings and particle size contribute and interact to produce observed diffraction phenomena. In contrast to cosine summation or matrix methods, where the number of terms to be considered increases geometrically with both the number of interlayer species and particle size, the α, β and γ variables are simply linear functions of the interlayer types. Calculations for 50 layer particles become no more difficult than five layer calculations. Finally, use of the equations derived in this paper allows the introduction of a wide variety of particle size distributions in a natural and easily handled manner with little increase in complexity over single particle size calculations.

Acknowledgements—The author wishes to express his appreciation to Dr. W. T. Granquist✝, who originally prompted the writing of this paper, for offering encouragement and advice and for spending many hours in the preparation of the figures. Thanks are also due to Dr. R. A. Rowland for critically reviewing the manuscript and to the Baroid Division of NL Industries for publication permission.

REFERENCES

Amil, A. R., Garcia, A. R. and MacEwan, D. M. C. (1967) *X-ray Diffraction Curves for the Analysis of Interstratified Structures*: Instituto de Quimica Inorganica, Volturna Press, Edinburgh, Scotland.

Hendricks, S. and Teller, E. (1942) X-ray interference in partially ordered layer lattices: *J. Chem. Phys.* **10,** 147–167.

Kakinoki, J. and Komura, Y. (1952) Intensity of X-ray diffraction by a one-dimensionally disordered crystal—I. General derivation in cases of the "Reichweite" $S = 0$ and 1: *J. Phys. Soc. Japan* **7,** 30–35.

MacEwan, D. M. C. (1958) Fourier transform methods for studying X-ray scattering from lamellar systems—II. The calculation of X-ray diffraction effects for various types of interstratification: *Kolloid Z.* **156**(1), 61–67.

MacEwan, D. M. C. and Amil, A. R. (1959) Fourier transform methods for studying X-ray scattering from lamellar systems—III. Some calculated diffraction effects of practical importance in clay mineral studies: *Kolloid Z.* **162**(2), 93–100.

Mering, J. (1949) L'interférence des rayons-X dans les systèmes a stratification désordonnée: *Acta Cryst.* **2,** 371–377.

Mering, J. (1950) Les réflexions des rayons-X par les minéraux argileux interstratifiés: *Trans. 4th Int. Cong. Soil Sci.* Amsterdam **3,** 21–26.

Reynolds, R. C. (1967) Interstratified clay systems: Calculation of the total one-dimensional diffraction function: *Am. Miner.* **52,** 661–672.

Rowland, R. A., Weiss, E. J. and Bradley, W. F. (1956) Dehydration of monoionic montmorillonites: *Proc. 4th Nat. Conf. Clays and Clay Minerals,* Nat. Acad. Sci. Publ. 456, 85–95.